Noisy evolution of graph-state entanglement

L. Aolita,[1] D. Cavalcanti,[2] R. Chaves,[3] C. Dhara,[1] L. Davidovich,[3] and A. Acín[1,4,*]

[1]*ICFO-Institut de Ciencies Fotoniques, Mediterranean Technology Park, E-08860 Castelldefels (Barcelona), Spain*
[2]*Centre for Quantum Technologies, University of Singapore, Singapore*
[3]*Instituto de Física, Universidade Federal do Rio de Janeiro, Caixa Postal 68528, 21941-972 Rio de Janeiro, RJ, Brazil*
[4]*ICREA-Institució Catalana de Recerca i Estudis Avançats, Lluis Companys 23, E-08010 Barcelona, Spain*

A general method for the study of the entanglement evolution of graph states under the action of Pauli maps was recently proposed in Cavalcanti *et al.* [Phys. Rev. Lett. **103**, 030502 (2009)]. This method is based on lower and upper bounds to the entanglement of the entire state as a function only of the state of a (typically) considerably smaller subsystem undergoing an effective noise process related to the original map. This provides a huge decrease in the size of the matrices involved in the calculation of entanglement in these systems. In the present paper we elaborate on this method in detail and generalize it to other natural situations not described by Pauli maps. Specifically, for Pauli maps we introduce an explicit formula for the characterization of the resulting effective noise. Beyond Pauli maps, we show that the same ideas can be applied to the case of thermal reservoirs at arbitrary temperature. In the latter case, we discuss how to optimize the bounds as a function of the noise strength. We illustrate our ideas with explicit exemplary results for several different graphs and particular decoherence processes. The limitations of the method are also discussed.

I. INTRODUCTION

Graph states [1] constitute an important family of genuine multiparticle-entangled states with several applications in quantum information. The most popular example of these are arguably the cluster states, which have been identified as a crucial resource for universal one-way measurement-based quantum computation [2,3]. Other members of this family were also proven to be potential resources for interesting tasks, as code words for quantum error correction [4], to implement secure quantum communication [5], or to simulate some aspects of the entanglement distribution of random states [6]. Moreover, graph states encompass the celebrated Greenberger-Horne-Zeilinger (GHZ) states [7], whose importance ranges from fundamental to applied issues. GHZ states can—for large-dimensional systems—be considered as simple models of the *gedanken* Schrödinger-cat states, are crucial for quantum communication protocols [8], and find applications in quantum metrology [9] and high-precision spectroscopy [10]. All these reasons explain the great deal of effort made both to theoretically understand [1] the properties of, and to generate and coherently manipulate, graph states in the laboratory [11].

For the same reasons, it is crucial to unravel the dynamics of graph states in realistic scenarios, where the system is unavoidably exposed to interactions with its environment and/or experimental imperfections. Previous studies on the robustness of graph-state entanglement in the presence of decoherence showed that the disentanglement times (i.e., the time for which the state becomes separable) increases with the system size [12,13]. However, the disentanglement time on its own is known not to provide in general a faithful figure of merit of the entanglement robustness; although the disentanglement time can grow with the number N of particles, the amount of entanglement in a given time can decay exponentially with

N [14]. The full dynamical evolution must then be monitored to draw any conclusions on the entanglement robustness.

A big obstacle must be overcome in the study of the entanglement robustness in general mixed states; the direct quantification of entanglement involves optimizations requiring computational resources that increase exponentially with N. The problem thus becomes in practice intractable even for relatively small system sizes, not to mention the direct assessment of entanglement during the entire noisy dynamics. All in all, some progress has been achieved in the latter direction for some very particular cases: For arbitrarily large linear-cluster states under collective dephasing, it is possible to calculate the exact value of the geometric measure of entanglement throughout the evolution [15]. In addition, bounds to the relative entropy and the global robustness of entanglement for two-colorable graph states [1] of any size under local dephasing were obtained in Ref. [16].

In a conceptually different approach, a framework to obtain families of lower and upper bounds to the entanglement evolution of graph—and graph-diagonal—states under decoherence was introduced in Ref. [17]. The bounds are obtained via a calculation that involves only the *boundary subsystem*, composed of the qubits lying at the boundary of the multipartition under scrutiny. This, very often, reduces considerably the size of the matrices involved in the calculation of entanglement. No optimization on the full system's parameter space is required throughout. Another remarkable feature of the method is that it is not limited to a particular entanglement quantifier but applies to all convex (bi-or multipartite) entanglement measures that do not increase under local operations and classical communication (LOCC). The latter are indeed two rather natural and general requirements [18,19].

In the case of open-dynamic processes described by Pauli maps, the lower and upper bounds coincide and the method thus allows one to calculate the exact entanglement of the noisy evolving state. Pauli maps encompass popular models of (independent or collective) noise, as depolarization, phase

----
*antonio.acin@icfo.es

flip, bit flip, and bit-phase flip errors, and are defined below. Moreover, one of the varieties of lower bounds is of extremely simple calculation and—despite less tight—depends only on the connectivity of the graph and not on its total size. The latter is a very advantageous property in situations where one wishes to assess the resistance of entanglement with growing system size. For example, the versatility of the formalism has very recently been demonstrated in Ref. [20], where it was applied to demonstrate the robustness of thermal bound entanglement in macroscopic many-body systems of spin-1/2 particles.

In the present paper, we elaborate on the details of the formalism introduced in [17]. For Pauli maps, we give an explicit formula for the characterization of the effective noise involved in the calculation of the bounds. Furthermore, we extend the method to the case where each qubit is subject to the action of independent thermal baths at arbitrary temperature. This is a crucial, realistic type of dynamic process that is not described by Pauli maps. In all cases, we exhaustively compare the different bounds with several concrete examples. Finally, we discuss the main advantages and limitations of our method in comparison with other approaches.

The article is organized as follows:

(1) Sec. II: Here we define the notation, introduce definitions, and review basic concepts required in the following sections. In particular, graph and graph-diagonal states are defined in Sec. II A and the noise models considered are presented in Sec. II B.

(2) Sec. III: A detailed description of the proposed framework is given in the context of fully general noises. Families of lower and upper bounds for the entanglement evolution in the particular multipartition of interest in terms of the entanglement of the boundary subsystem alone under an effective noise are provided.

(3) Sec. IV: The developed machinery is applied to the case of noises described by arbitrary Pauli maps and by diffusion and dissipation with independent thermal reservoirs at any temperature. Exact results for the entanglement decay are obtained for Pauli maps, whereas optimized bounds are provided in the other cases.

(4) Sec. V: We first discuss how the method can be extended to other initial states or decoherence processes. In particular, how nontight lower bounds for the entanglement evolution of *any* initial state subjected to *any* decoherence process can be obtained. Then we comment on the limitations of the method.

(5) Sec. VI: We conclude the paper with a summary of the results and their physical implications.

II. BASIC CONCEPTS

In this section, we define graph and graph-diagonal states, and introduce the basics of open-system dynamics and the particular noise models used later.

A. Graph and graph-diagonal states

Qubit graph states are multiqubit quantum states defined from mathematical graphs through the rule described in the following. First, a mathematical graph $G_{(\mathcal{V},\mathcal{C})} \equiv \{\mathcal{V},\mathcal{C}\}$ is defined by a set $\mathcal{V}$ of N vertices, or nodes, and a set $\mathcal{C}$, of connections, or edges, connecting each node i to some other j.
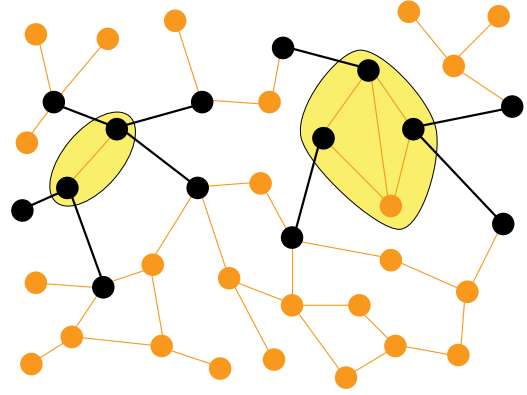

FIG. 1. (Color online) Mathematical graph associated with a given physical graph state. An exemplary bipartition divides the system into two subparts: the yellow and white regions. The edges in black are the *boundary-crossing edges* $\mathcal{X}$ and the nodes (also in black) connected by them are the *boundary nodes* $\mathcal{Y}$. Together they compose the *boundary subgraph* $G(\mathcal{Y},\mathcal{X})$. The remaining vertices, painted in orange, constitute the *nonboundary subsystem*.

An example of such a graph is illustrated in Fig. 1. Each vertex $i \in \mathcal{V}$ represents a qubit in the associated physical system, and each edge $\{i,j\} \in \mathcal{C}$ represents a unitary maximally entangling controlled-Z (CZ) gate, $\mathrm{CZ}_{ij} = |0_i 0_j\rangle\langle 0_i 0_j| + |0_i 1_j\rangle\langle 0_i 1_j| + |1_i 0_j\rangle\langle 1_i 0_j| - |1_i 1_j\rangle\langle 1_i 1_j|$, between the qubits i and j connected through the corresponding edge. The N-qubit graph state $|G_{(\mathcal{V},\mathcal{C})_0}\rangle$ corresponding to graph $G_{(\mathcal{V},\mathcal{C})}$ is then operationally defined as follows:

(i) Initialize every qubit i in the superposition $|+_i\rangle = \frac{1}{\sqrt{2}}(|0_i\rangle + |1_i\rangle)$, so that the joint state is in the product state $|g_{(\mathcal{V})_0}\rangle \equiv \bigotimes_{i \in \mathcal{V}} |+_i\rangle$.

(ii) Then, for every connection $\{i,j\} \in \mathcal{C}$ apply the gate CZ_{ij} to $|g_{(\mathcal{V})_0}\rangle$. That is,

$$\left|G_{(\mathcal{V},\mathcal{C})_0}\right\rangle = \bigotimes_{\{i,j\}\in\mathcal{C}} \mathrm{CZ}_{ij}\left|g_{(\mathcal{V})_0}\right\rangle. \tag{1}$$

Graph state (1) can also be defined in an alternative, nonoperational fashion. Associated to each node $i \in \mathcal{V}$ of a given graph $G_{(\mathcal{V},\mathcal{C})}$ we define the operator,

$$S_i \equiv X_i \bigotimes_{j\in\mathcal{N}_i} Z_j, \tag{2}$$

with X_i and Z_j the usual Pauli operators acting, respectively, on qubits i and j, and where $\mathcal{N}_i$ denotes the set of neighbors of i, directly connected to it by an edge $\{i,j\}$. Operator (2) possesses eigenvalues 1 and -1. It is the ith generator of the stabilizer group and is often called for short the *stabilizer operator*. All N stabilizer operators commute and share, therefore, a common basis of eigenstates. Graph state $|G_{(\mathcal{V},\mathcal{C})_0}\rangle$ in turn has the peculiarity of being the unique common eigenstate of eigenvalue $+1$ [1]. In other words,

$$S_i\left|G_{(\mathcal{V},\mathcal{C})_0}\right\rangle = \left|G_{(\mathcal{V},\mathcal{C})_0}\right\rangle \forall\, i \in \mathcal{V}.$$

The other $2^N - 1$ common eigenstates $|G_{(\mathcal{V},\mathcal{C})_v}\rangle$ are in turn related to (1) by a local unitary operation:

$$\left|G_{(\mathcal{V},\mathcal{C})_v}\right\rangle = \bigotimes_{i\in\mathcal{V}} Z_i^{v_i}\left|G_{(\mathcal{V},\mathcal{C})_0}\right\rangle \equiv Z^v\left|G_{(\mathcal{V},\mathcal{C})_0}\right\rangle, \tag{3}$$

such that $S_i|G_{(\mathcal{V},\mathcal{C})_\nu}\rangle = (-1)^{\nu_i}|G_{(\mathcal{V},\mathcal{C})_\nu}\rangle$, where ν is a multi-index representing the binary string $\nu \equiv \nu_1 \cdots \nu_N$, with $\nu_i = 0$ or $1 \ \forall \ i \in \mathcal{V}$, and where the shorthand notation $Z^\nu \equiv \bigotimes_{i\in\mathcal{V}} Z_i^{\nu_i}$ has been introduced. Therefore, states (3) possess all exactly the same entanglement properties and, together with $|G_{(\mathcal{V},\mathcal{C})_0}\rangle$, define a complete orthonormal basis of $\mathcal{H}$, called the graph-state basis of $\mathcal{H}$ (corresponding to the graph $G_{(\mathcal{V},\mathcal{C})}$). Any state ρ diagonal in such a basis is called a *graph-diagonal state*:

$$\rho_{\text{GD}} = \sum_\nu P_\nu |G_{(\mathcal{V},\mathcal{C})_\nu}\rangle\langle G_{(\mathcal{V},\mathcal{C})_\nu}|, \tag{4}$$

where P_ν is any probability distribution. Interestingly, for any graph, any arbitrary N-qubit state can always be depolarized by some separable map (defined below) into the form (4) without changing its diagonal elements in the considered graph basis [21].

Two simple identities following from definition (2) will be crucial for our purposes. For every eigenstate $|G_{(\mathcal{V},\mathcal{C})_\nu}\rangle$ of S_i, with eigenvalues $s_{i\nu} = 1$ or -1,

$$X_i|G_{(\mathcal{V},\mathcal{C})_\nu}\rangle = S_i \otimes \bigotimes_{j\in\mathcal{N}_i} Z_j |G_{(\mathcal{V},\mathcal{C})_\nu}\rangle = s_{i\nu} \bigotimes_{j\in\mathcal{N}_i} Z_j |G_{(\mathcal{V},\mathcal{C})_\nu}\rangle, \tag{5}$$

where definition (2) was used, and

$$Y_i|G_{(\mathcal{V},\mathcal{C})_\nu}\rangle = (-i)Z_i.S_i \otimes \bigotimes_{j\in\mathcal{N}_i} Z_j |G_{(\mathcal{V},\mathcal{C})_\nu}\rangle$$
$$= s_{i\nu}(-i)Z_i \otimes \bigotimes_{j\in\mathcal{N}_i} Z_j |G_{(\mathcal{V},\mathcal{C})_\nu}\rangle. \tag{6}$$

So, when applied to any pure graph—or mixed graph-diagonal—state, the following operator equivalences hold up to a global phase:

$$X_i \leftrightarrow \bigotimes_{j\in\mathcal{N}_i} Z_j, \tag{7a}$$

$$Y_i \leftrightarrow Z_i \otimes \bigotimes_{j\in\mathcal{N}_i} Z_j. \tag{7b}$$

B. Open-system dynamics

As we mentioned in Sec. I, our ultimate goal is to study the behavior of graph-state entanglement in realistic dynamic scenarios where the system evolves during a time interval t according to a generic physical process, which can include decoherence. This process can always be represented by a completely positive trace-preserving map Λ, that maps any initial state ρ to the evolved one after a time t, $\rho_t \equiv \Lambda(\rho)$. In turn, for every such Λ, there always exists a maximum of D^2 [$D = \dim(\mathcal{H})$] operators K_μ such that the map is expressed in the Kraus form [22]:

$$\rho_t \equiv \Lambda(\rho) = \sum_\mu K_\mu \rho K_\mu^\dagger. \tag{8}$$

Operators K_μ are called the Kraus operators, and decompose the identity operator $\mathbf{1}$ of $\mathcal{H}$ in the following manner: $\sum_\mu K_\mu^\dagger K_\mu = \mathbf{1}$. Conversely, the Kraus representation encapsulates all possible physical dynamics of the system. That is, any map expressible as in (8) is automatically completely

positive and trace preserving. For our case of interest (N-qubit systems), index μ runs from 0 to $(2^N)^2 - 1 = 4^N - 1$. For later convenience, we will represent it in base 4, decomposing it as the following multi-index: $\mu \equiv \mu_1 \cdots \mu_N$, with $\mu_i = 0$, 1, 2, or 3 $\forall \ i \in \mathcal{V}$.

We call Λ a separable map with respect to some multi-partition of the system if each and all of its Kraus operators factorize as tensor products of local operators each one with support on only one of the subparts. For example, if we split the qubits associated with the graph shown in Fig. 1 into a set $\mathcal{Y}$ of *boundary qubits* (in black) and its complement $\overline{\mathcal{Y}} \equiv \mathcal{V}/\mathcal{Y}$ of *nonboundary qubits* (in green), Λ is separable with respect to this partitioning if $K_\mu \equiv K_{\mathcal{Y}_\mu} \otimes K_{\overline{\mathcal{Y}}_\mu}$, with $K_{\mathcal{Y}_\mu}$ and $K_{\overline{\mathcal{Y}}_\mu}$ operators acting nontrivially only on the Hilbert spaces of the boundary and nonboundary qubits, respectively.

In turn, we call Λ an *independent map* with respect to some multipartition of the system if it can be factorized as the composition (tensor product) of individual maps acting independently on each subpart. Otherwise, we say that Λ is a *collective map*. Examples of *fully independent maps* are those in which each qubit i is independently subject to its own local noise channel $\mathcal{E}_i$. By the term *independent map* without explicit mention to any respective multipartition we will refer throughout to fully independent maps. In this case, the global map Λ factorizes completely:

$$\Lambda(\rho) = \mathcal{E}_1 \otimes \mathcal{E}_2 \otimes \cdots \otimes \mathcal{E}_N(\rho). \tag{9}$$

It is important to notice that all independent maps are necessarily separable but a general separable map does not need to be factorable as in (9) and can therefore be both, either individual or collective.

1. Pauli maps

A crucial family of fully separable maps is that of the *Pauli maps*, for which every Kraus operator is proportional to a product of individual Pauli and identity operators acting on each qubit. That is, $K_\mu \equiv \sqrt{P_{(\mu_1,\ldots\mu_N)}} \ \sigma_{1\mu_1} \otimes \cdots \otimes \sigma_{N\mu_N} \equiv \sqrt{P_\mu} \ \sigma_\mu$, with $\sigma_{i0} = \mathbf{1}_i$ (the identity operator on qubit i), $\sigma_{i1} = X_i$, $\sigma_{i2} = Y_i$, and $\sigma_{i3} = Z_i$, and $P_{(\mu_1,\ldots\mu_N)} \equiv P_\mu$ any probability distribution. Popular instances are the (collective or independent) depolarization and dephasing (also called phase damping, or phase-flip) maps, and the (individual) bit-flip and bit-phase-flip channels [22]. For example, the independent depolarizing (D) channel describes the situation in which the qubit remains untouched with probability $1 - p$, or is depolarized—meaning that it is taken to the maximally mixed state (white noise)—with probability p. It is characterized by the fully factorable probability $P_\mu = p_{1\mu_1} \times \cdots p_{N\mu_N}$, with $p_{i0} = 1 - p$ and $p_{i1} = p_{i2} = p_{i3} = p/3$, $\forall \ i \in \mathcal{V}$. The independent phase-damping (PD) channel in turn induces the complete loss of quantum coherence with probability p, but without any energy (population) exchange. It is also given by a fully factorable probability with $p_{i0} = 1 - p/2$, $p_{i1} = 0 = p_{i2}$, and $p_{i3} = p/2$, $\forall \ i \in \mathcal{V}$.

For later convenience, we finally recall that each Pauli operator $\sigma_{i\mu_i}$ can be written in the following way: $T_{i(u_i,v_i)} \equiv Z_i^{v_i}.X_i^{u_i}$, with u_i and $v_i = 0$, or 1. Indeed, notice that $\sigma_{i\,2v_i+|v_i+u_i|_2} = T_{i(u_i,v_i)}$ (up to an irrelevant phase factor for $u_i = 1 = v_i$), where "$|\ |_2$" stands for modulo 2. In

this representation, called the *chord representation* [23], the Kraus decomposition of the previously considered general Pauli map has the following Kraus operators: $K_{C(U,V)} \equiv \sqrt{P_{C(u_1,v_1,\ldots u_N,v_N)}}$ $T_{1(u_1,v_1)} \otimes \cdots \otimes T_{N(u_N,v_N)} \equiv \sqrt{P_{C(U,V)}} \ T_{(U,V)}$, where $U \equiv (u_1, \ldots u_N)$ and $V \equiv (v_1, \ldots v_N)$. The probability $P_{C(U,V)} \equiv P_{C(u_1,v_1,\ldots u_N,v_N)}$ in turn is related to the original P_μ by $P_{C(u_1,v_1,\ldots u_N,v_N)} \equiv P_{(2v_1+|v_1+u_1|_2,\ldots,2v_N+|v_N+u_N|_2)}$.

2. Independent thermal baths

An important example of a non-Pauli, independent map is the generalized amplitude-damping channel (GAD) [22]. It represents energy diffusion and dissipation with a thermal bath into which each qubit is individually immersed. Its Kraus representation is

$$K_{i\,\mu_i=0} \equiv \sqrt{\frac{\bar{n}+1}{2\bar{n}+1}}(|0_i\rangle\langle 0_i| + \sqrt{1-p}|1_i\rangle\langle 1_i|), \quad (10a)$$

$$K_{i\,\mu_i=1} \equiv \sqrt{\frac{\bar{n}+1}{2\bar{n}+1}}\,p|0_i\rangle\langle 1_i|, \quad (10b)$$

$$K_{i\,\mu_i=2} \equiv \sqrt{\frac{\bar{n}}{2\bar{n}+1}}(\sqrt{1-p}|0_i\rangle\langle 0_i| + |1_i\rangle\langle 1_i|), \quad (10c)$$

and

$$K_{i\,\mu_i=3} \equiv \sqrt{\frac{\bar{n}}{2\bar{n}+1}}\,p|1_i\rangle\langle 0_i|. \quad (10d)$$

Here $\bar{n}$ is the average number of quanta in the thermal bath, $p \equiv p(t) \equiv 1 - e^{-\frac{1}{2}\gamma(2\bar{n}+1)t}$ is the probability of the qubit exchanging a quantum with the bath after a time t, and γ is the zero-temperature dissipation rate. Channel GAD is actually the extension to finite temperature of the purely dissipative amplitude damping (AD) channel, which is obtained from GAD in the zero-temperature limit $\bar{n} = 0$. In the opposite extreme, the purely diffusive case is obtained from GAD in the composite limit $\bar{n} \to \infty$, $\gamma \to 0$, and $\bar{n}\gamma = \Gamma$, where Γ is the diffusion constant. Note that in the purely diffusive limit, channel GAD becomes a Pauli channel, with defining individual probabilities $p_{i0} = \frac{1}{2}(1 - p/2 + \sqrt{1-p})$, $p_{i1} = \frac{p}{4} = p_{i2}$, and $p_{i3} = \frac{1}{2}(1 - p/2 - \sqrt{1-p})$, $\forall i \in \mathcal{V}$.

Finally, the probability p in channels D, PD, and GAD above can be interpreted as a convenient parametrization of time, where $p = 0$ refers to the initial time 0 and $p = 1$ refers to the asymptotic limit $t \to \infty$.

III. EVOLUTION OF GRAPH-STATE ENTANGLEMENT UNDER GENERIC NOISE

As mentioned before, the direct calculation of the entanglement in arbitrary mixed states is a task exponentially hard in the system's size [19]. In this section, we elaborate in detail a formalism that dramatically simplifies this task for graph—or graph-diagonal—states undergoing a noisy evolution in a fully general context. Along the way, we also describe carefully which requirements an arbitrary noisy map has to satisfy so that the formalism can be applied.

A. The general idea

Consider a system initially in graph state (1) that evolves during a time t according to the general map (8) toward the evolved state,

$$\rho_t \equiv \Lambda\big(|G_{(\mathcal{V},\mathcal{C})_0}\rangle\big) = \sum_\mu K_\mu |G_{(\mathcal{V},\mathcal{C})_0}\rangle\langle G_{(\mathcal{V},\mathcal{C})_0}|K_\mu^\dagger. \quad (11)$$

We would like to follow the entanglement $E(\rho_t)$ of ρ_t during its entire evolution. Here, E is any convex entanglement monotone [18,19] that quantifies the entanglement content in some given multipartition of the system. An example of such multipartition is displayed in Fig. 1, where the associated graph is split into two subsets, painted, respectively, in yellow and white in the figure. The edges that connect vertices at different subsets are called the *boundary-crossing edges* and are painted in black in the figure. We call the set of all the boundary-crossing edges $\mathcal{X} \subseteq \mathcal{C}$, and its complement $\overline{\mathcal{X}} \equiv \mathcal{C}/\mathcal{X}$ the set of all non-boundary-crossing edges. All the qubits associated with vertices connected by any edge in $\mathcal{X}$ constitute the set $\mathcal{Y} \subseteq \mathcal{V}$ of *boundary qubits* (or *boundary subsystem*), and its complement $\overline{\mathcal{Y}} \equiv \mathcal{V}/\mathcal{Y}$ is the nonboundary qubit set. We refer to $G_{(\mathcal{Y},\mathcal{X})}$ as the *boundary subgraph*.

We can use this classification and the operational definition (1) to write the initial graph state as

$$|G_{(\mathcal{V},\mathcal{C})_0}\rangle = \bigotimes_{\{i,j\}\in\overline{\mathcal{X}}} \mathrm{CZ}_{ij} |G_{(\mathcal{Y},\mathcal{X})_0}\rangle \otimes |g_{(\overline{\mathcal{Y}})_0}\rangle, \quad (12)$$

where $|g_{(\overline{\mathcal{Y}})_0}\rangle \equiv \bigotimes_{i\in\overline{\mathcal{Y}}} |+_i\rangle$. In other words, we explicitly factor all the CZ gates corresponding to non-boundary-crossing edges out.

Consider now the application of some Kraus operator K_μ of a general map on graph state (12): $K_\mu \bigotimes_{\{i,j\}\in\overline{\mathcal{X}}} \mathrm{CZ}_{ij}|G_{(\mathcal{Y},\mathcal{X})_0}\rangle \otimes |g_{(\overline{\mathcal{Y}})_0}\rangle$. The latter can always be written as $\bigotimes_{\{i,j\}\in\overline{\mathcal{X}}} \mathrm{CZ}_{ij}\tilde{K}_\mu|G_{(\mathcal{Y},\mathcal{X})_0}\rangle \otimes |g_{(\overline{\mathcal{Y}})_0}\rangle$, with

$$\tilde{K}_\mu = \bigotimes_{\{i,j\}\in\overline{\mathcal{X}}} \mathrm{CZ}_{ij}\, K_\mu \bigotimes_{\{i',j'\}\in\overline{\mathcal{X}}} \mathrm{CZ}_{i'j'}, \ \forall\,\mu. \quad (13)$$

Now, consider every map Λ such that transformation rule (13) yields, for each μ, modified Kraus operators of the form,

$$\tilde{K}_\mu = \tilde{K}_{\mathcal{Y}\gamma} \otimes \tilde{K}_{\overline{\mathcal{Y}}\omega}, \quad (14)$$

where $\tilde{K}_{\mathcal{Y}\gamma}$ and $\tilde{K}_{\overline{\mathcal{Y}}\omega}$ are normalized modified Kraus operators acting nontrivially only on the boundary and nonboundary qubits, respectively. In the last, $\gamma = \{\mu_i, i \in \mathcal{Y}\}$ and $\omega = \{\mu_i, i \in \overline{\mathcal{Y}}\}$ are multi-indices labeling, respectively, the alternatives for the boundary and nonboundary subsystems, being μ_i in turn the individual base-4 indices introduced after Eq. (8). The modified map $\tilde{\Lambda}$, composed of Kraus operators $\tilde{K}_\mu$ is then clearly biseparable with respect to the bipartition "boundary/nonboundary". For all such maps the calculation of $E(\rho_t)$ can be drastically simplified, as we see in what follows.

In these cases, the evolved state (11) can be written as

$$\rho_t \equiv \Lambda\big(|G_{(\mathcal{V},\mathcal{C})_0}\rangle\big) = \bigotimes_{\{i,j\}\in\overline{\mathcal{X}}} \mathrm{CZ}_{ij}\, \tilde{\rho}_t \bigotimes_{\{k,l\}\in\overline{\mathcal{X}}} \mathrm{CZ}_{kl}, \quad (15)$$

with

$$
\begin{aligned}
\tilde{\rho}_t &= \tilde{\Lambda}\big(|G_{(\mathcal{Y},\mathcal{X})_0}\rangle \otimes |g_{(\overline{\mathcal{Y}})_0}\rangle\big) \\
&= \sum_\mu \tilde{K}_{\mathcal{Y}\gamma(\mu)}|G_{(\mathcal{Y},\mathcal{X})_0}\rangle\langle G_{(\mathcal{Y},\mathcal{X})_0}|\tilde{K}^\dagger_{\mathcal{Y}\gamma(\mu)} \\
&\quad \otimes \tilde{K}_{\overline{\mathcal{Y}}\omega(\mu)}|g_{(\overline{\mathcal{Y}})_0}\rangle\langle g_{(\overline{\mathcal{Y}})_0}|\tilde{K}^\dagger_{\overline{\mathcal{Y}}\omega(\mu)} \\
&= \sum_\omega \tilde{K}_{\overline{\mathcal{Y}}\omega}|g_{(\overline{\mathcal{Y}})_0}\rangle\langle g_{(\overline{\mathcal{Y}})_0}|\tilde{K}^\dagger_{\overline{\mathcal{Y}}\omega} \\
&\quad \otimes \sum_\gamma \tilde{K}_{\mathcal{Y}(\gamma|\omega)}|G_{(\mathcal{Y},\mathcal{X})_0}\rangle\langle G_{(\mathcal{Y},\mathcal{X})_0}|\tilde{K}^\dagger_{\mathcal{Y}(\gamma|\omega)}, \quad (16)
\end{aligned}
$$

where $\tilde{K}_{\mathcal{Y}(\gamma|\omega)}$ is the γth modified Kraus operator on the boundary subsystem given that $\tilde{K}_{\overline{\mathcal{Y}}\omega}$ has been applied to the nonboundary one. Recall that both $\gamma \equiv \gamma(\mu)$ and $\omega \equiv \omega(\mu)$ come from the same single multi-index μ and are therefore in general not independent on one another. In the second equality of (16) we have chosen to treat ω as an independent variable for the summation and make γ explicitly depend on ω. This can always be done and will be convenient for our purposes.

The crucial observation now is that the CZ operators explicitly factored out in the evolved state (15) correspond to non-boundary-crossing edges. Thus, they act as *local unitary operations* with respect to the multipartition of interest. For this reason, and since local unitary operations do not change the entanglement content of any state, the equivalence,

$$
E(\rho_t) = E(\tilde{\rho}_t), \quad (17)
$$

holds.

In the forthcoming subsections we see how, by exploiting this equivalence in different noise scenarios, the computational effort required for a reliable estimation (and in some cases, an exact calculation) of $E(\rho_t)$ can be considerably reduced. The main idea behind this reduction lies on the fact that, whereas in general state (11) the entanglement can be distributed among all particles in the graph, in state (16) the boundary and nonboundary subsystems are explicitly in a separable state. All the entanglement in the multipartition of interest is therefore localized exclusively in the boundary subgraph. The situation is graphically represented in Fig. 2, where the same graph as in Fig. 1 is plotted but with all its non-boundary-crossing edges erased.
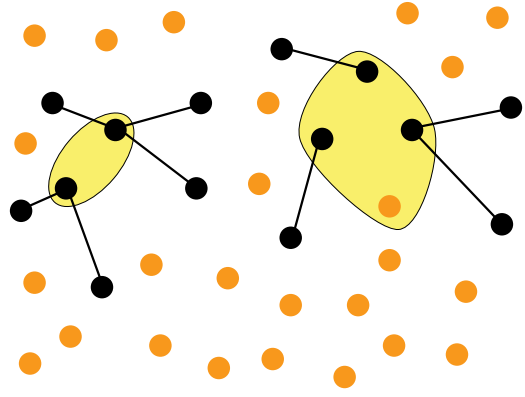

FIG. 2. (Color online) Same graph as in Fig. 1 but where all non-boundary-crossing edges have been erased, representing the fact that the boundary and nonboundary subsystems are fully unentangled. The entanglement in the whole system is obtained via a calculation involving only the smaller boundary subsystem.

More precisely, the general approach consists of obtaining lower and upper bounds on $E(\rho_t)$ by bounding the entanglement of state (16) from above and below as explained in what follows.

1. Lower bounds to the entanglement evolution

The property of LOCC monotonicity of E, which means that the average entanglement cannot grow during an LOCC process [18], allows us to derive lower bounds on $E(\tilde{\rho}_t)$. The ones we consider can be obtained by the following generic procedure:

(i) After bringing the studied state into the form (16), apply some local general measurement $M = \{M_\omega\}$, with measurement elements M_ω, on the non-boundary subsystem $\overline{\mathcal{Y}}$;

(ii) for each measurement outcome ω trace out the measured nonboundary subsystem;

(iii) and, finally, calculate the mean entanglement in the resulting state of the boundary subsystem $\mathcal{Y}$, averaged over all outcomes ω.

Since this procedure constitutes an LOCC with respect to the multipartition under scrutiny, the latter average entanglement can only be smaller than, or equal to, that of the initial state, that is,

$$
E(\rho_t) = E(\tilde{\rho}_t) \geqslant \sum_\omega P_\omega E\left(\sum_{\omega'} \frac{1}{P_\omega}\langle g_{(\overline{\mathcal{Y}})_0}|\tilde{K}^\dagger_{\overline{\mathcal{Y}}\omega'}M^\dagger_\omega.M_\omega\tilde{K}_{\overline{\mathcal{Y}}\omega'}|g_{(\overline{\mathcal{Y}})_0}\rangle \sum_\gamma \tilde{K}_{\mathcal{Y}(\gamma|\omega')}|G_{(\mathcal{Y},\mathcal{X})_0}\rangle\langle G_{(\mathcal{Y},\mathcal{X})_0}|\tilde{K}^\dagger_{\mathcal{Y}(\gamma|\omega')}\right), \quad (18)
$$

with $P_\omega \equiv \sum_{\omega'}\langle g_{(\overline{\mathcal{Y}})_0}|\tilde{K}^\dagger_{\overline{\mathcal{Y}}\omega'}M^\dagger_\omega.M_\omega\tilde{K}_{\overline{\mathcal{Y}}\omega'}|g_{(\overline{\mathcal{Y}})_0}\rangle$ being the probability of outcome ω.

Notice that if the states $\{\tilde{K}_{\overline{\mathcal{Y}}\omega'}|g_{(\overline{\mathcal{Y}})_0}\rangle\}$ of the nonboundary subsystem happen to be orthogonal, then there exists an optimal measurement $M = \{M_\omega \equiv \frac{\tilde{K}_{\overline{\mathcal{Y}}\omega}|g_{(\overline{\mathcal{Y}})_0}\rangle\langle g_{(\overline{\mathcal{Y}})_0}|\tilde{K}^\dagger_{\overline{\mathcal{Y}}\omega}}{\langle g_{(\overline{\mathcal{Y}})_0}|\tilde{K}^\dagger_{\overline{\mathcal{Y}}\omega}\tilde{K}_{\overline{\mathcal{Y}}\omega}|g_{(\overline{\mathcal{Y}})_0}\rangle}\}$ that can distinguish them unambiguously, so

that $\langle g_{(\overline{\mathcal{Y}})_0}|\tilde{K}^\dagger_{\overline{\mathcal{Y}}\omega'}M^\dagger_\omega.M_\omega\tilde{K}_{\overline{\mathcal{Y}}\omega'}|g_{(\overline{\mathcal{Y}})_0}\rangle = \delta_{\omega,\omega'} \times \langle g_{(\overline{\mathcal{Y}})_0}|\tilde{K}^\dagger_{\overline{\mathcal{Y}}\omega}\tilde{K}_{\overline{\mathcal{Y}}\omega}|g_{(\overline{\mathcal{Y}})_0}\rangle$ and $P_\omega = \langle g_{(\overline{\mathcal{Y}})_0}|\tilde{K}^\dagger_{\overline{\mathcal{Y}}\omega}\tilde{K}_{\overline{\mathcal{Y}}\omega}|g_{(\overline{\mathcal{Y}})_0}\rangle$. In these cases an optimal lower bound is achieved as

$$
E(\rho_t) \geqslant \sum_\omega P_\omega E\left(\sum_\gamma \tilde{K}_{\mathcal{Y}(\gamma|\omega)}|G_{(\mathcal{Y},\mathcal{X})_0}\rangle\langle G_{(\mathcal{Y},\mathcal{X})_0}|\tilde{K}^\dagger_{\mathcal{Y}(\gamma|\omega)}\right). \quad (19)
$$

Full distinguishability of the states in the nonboundary subsystem allows to reduce the mixing in the remaining boundary subsystem. In other words, the measurement outcome ω works as a perfect *flag* that marks which subensemble of states of the boundary subsystem, from all those present in mixture (16), corresponds indeed to the obtained outcome.

In the opposite extreme, when states $\{\tilde{K}_{\overline{y}_{\omega'}}|g_{(\overline{y})_0}\rangle\}$ are all equal, no flagging information can be obtained via any measurement. In this case, the resulting bound is always equal to that obtained had we not made any measurement at all, but just directly taken the partial trace over $\overline{\mathcal{Y}}$ from (16):

$$E(\rho_t) \geqslant E\left(\frac{1}{2^{|\overline{\mathcal{Y}}|}}\sum_{\omega,\gamma}\tilde{K}_{\mathcal{Y}(\gamma|\omega)}|G_{(\mathcal{Y},\mathcal{X})_0}\rangle\langle G_{(\mathcal{Y},\mathcal{X})_0}|\tilde{K}^{\dagger}_{\mathcal{Y}(\gamma|\omega)}\right),$$
$$(20)$$

where $|\overline{\mathcal{Y}}|$ stands for the number of nonboundary qubits and full mixing over variable ω takes place now.

Henceforth, we refer to lower bound (20) as the *lowest lower bound* (LLB). As its name suggests, its tightness is far from the optimal one given by (19). However, as we will see in the forthcoming subsections, due to the partial tracing, it typically does not depend on the total system's size but just on that of the boundary subsystem.

This constitutes an appealing, useful property, for it allows one to draw generic conclusions about the robustness of entanglement in certain partitions of graph states, irrespective of their number of constituent particles (see examples in Sec. IV B).

2. Upper bounds to the entanglement evolution

On the other hand, we consider upper-bounds on $E(\rho_t)$ based on the property of convexity of E, which essentially means that the entanglement of the convex sum is lower than, or equal to, the convex sum of the entanglements [18,19]. From (16), the latter implies that

$$E(\rho_t) = E(\tilde{\rho}_t) \leqslant \sum_{\omega} P_{\omega} E\left(\frac{1}{P_{\omega}}\tilde{K}_{\overline{y}_{\omega}}|g_{(\overline{y})_0}\rangle\langle g_{(\overline{y})_0}|\tilde{K}^{\dagger}_{\overline{y}_{\omega}}\right.$$

$$\left.\otimes \sum_{\gamma}\tilde{K}_{\mathcal{Y}(\gamma|\omega)}|G_{(\mathcal{Y},\mathcal{X})_0}\rangle\langle G_{(\mathcal{Y},\mathcal{X})_0}|\tilde{K}^{\dagger}_{\mathcal{Y}(\gamma|\omega)}\right), \quad (21)$$

where, once again, $P_{\omega} = \langle g_{(\overline{y})_0}|\tilde{K}^{\dagger}_{\overline{y}_{\omega}}\tilde{K}_{\overline{y}_{\omega}}|g_{(\overline{y})_0}\rangle$. In each term of the last summation the boundary and nonboundary subsystems inside the brackets are in a *product state*. Therefore, as for what the multipartition of interest concerns, the nonboundary subsystem works as a locally added ancilla (in a state $\frac{1}{P_{\omega}}\tilde{K}_{\overline{y}_{\omega}}|g_{(\overline{y})_0}\rangle\langle g_{(\overline{y})_0}|\tilde{K}^{\dagger}_{\overline{y}_{\omega}}$) and consequently does not have any influence on the amount of entanglement. This leads to the generic upper bound,

$$E(\rho_t) \leqslant \sum_{\omega} P_{\omega} E\left(\sum_{\gamma}\tilde{K}_{\mathcal{Y}(\gamma|\omega)}|G_{(\mathcal{Y},\mathcal{X})_0}\rangle\langle G_{(\mathcal{Y},\mathcal{X})_0}|\tilde{K}^{\dagger}_{\mathcal{Y}(\gamma|\omega)}\right).$$
$$(22)$$

3. Exact entanglement

Notice that the upper bound (22) and the optimal lower bound (19) coincide. This means that, in the previously mentioned case when states $\{\tilde{K}_{\overline{y}_{\omega}}|g_{(\overline{y})_0}\rangle\}$ are orthogonal, these coincident bounds yield actually the exact value of $E(\rho_t)$:

$$E(\rho_t) = \sum_{\omega} P_{\omega} E\left(\sum_{\gamma}\tilde{K}_{\mathcal{Y}(\gamma|\omega)}|G_{(\mathcal{Y},\mathcal{X})_0}\rangle\langle G_{(\mathcal{Y},\mathcal{X})_0}|\tilde{K}^{\dagger}_{\mathcal{Y}(\gamma|\omega)}\right).$$
$$(23)$$

Expression (23) is still not an analytic closed formula for the exact entanglement of ρ_t, but reduces its calculation to that of the average entanglement over an ensemble of states of the boundary subsystem alone. More in detail, a brute-force calculation of $E(\rho_t)$ would require, in general, a convex optimization over the entire $2^{2N} - 1$ real-parameter space. Through Eq. (23), in turn, such a calculation is reduced to that of the average entanglement over a sample of $2^{|\overline{\mathcal{Y}}|}$ states (one for each ω) of $|\mathcal{Y}|$ qubits, being $|\mathcal{Y}|$ the number of boundary qubits. The latter involves at most $2^{|\overline{\mathcal{Y}}|}$ independent optimizations over a $2^{2|\mathcal{Y}|} - 1$ real-parameter space. This, from the point of view of computational memory required, accounts for a reduction of resources by a factor of $O(2^{2|\overline{\mathcal{Y}}|})$. Alternatively, when computational memory is not a major restriction, for example, if large classical-computer clusters are at hand, one can take advantage of the fact that the $|\overline{\mathcal{Y}}|$ required optimizations in (23) are independent and therefore the calculation comes readily perfectly suited for parallel computing.

In the cases where states $\{\tilde{K}_{\overline{y}_{\omega}}|g_{(\overline{y})_0}\rangle\}$ are not orthogonal and the upper and lower bounds do not coincide, expressions (22) and (18) still yield highly nontrivial upper and lower bounds, respectively, as we discuss in Sec. IV B.

Finally, it is important to stress that all the bounds derived here are general in the sense that they hold for any function fulfilling the fundamental properties of convexity and monotonicity under LOCC processes. This class includes genuine multipartite entanglement measures, as well as several quantities designed to quantify the usefulness of quantum states in the fulfillment of some given task for quantum-information processing or communication [19].

IV. GRAPH STATES UNDER PAULI MAPS OR THERMAL RESERVOIRS

In the present section we apply the ideas of the previous section to some important concrete examples of noise processes. This shows how the method is helpful in the entanglement calculation for systems in natural, dynamic physical scenarios. We first discuss the case of Pauli maps and then the generalized amplitude damping channel (thermal reservoir). Explicit calculations for noisy graph states composed of up to 14 qubits are presented as examples.

A. Pauli maps on graph states

Pauli maps defined in Sec. II B provide the most important and general subfamily of noise types for which expression (23)

for the exact entanglement of the evolved state applies. In this case, every X_i or Y_i Pauli matrix in the map's Kraus operators is systematically substituted by products of Z_i and $\mathbf{1}_i$ according to rules (7). The resulting map $\tilde{\Lambda}$ defined in this way automatically commutes with any CZ gate and is fully separable, so that condition (14) is trivially satisfied. Since for every qubit in the system four orthogonal single qubit operators are mapped into products of just two, several different Kraus operators of the original map contribute to the same Kraus operator of the modified one. This allows us to simplify the notation going from indices μ_i, which run over four possible values each, to modified indices $\tilde{\mu}_i$ having only two different alternatives. In fact, the original operators K_μ give rise to only 2^N modified ones of the form,

$$\tilde{K}_{\tilde{\mu}} = \sqrt{\tilde{P}_{\tilde{\mu}}} Z_1^{\tilde{\mu}_1} \otimes Z_2^{\tilde{\mu}_2} \otimes \cdots \otimes Z_N^{\tilde{\mu}_N} \equiv \sqrt{\tilde{P}_{\tilde{\mu}}} Z^{\tilde{\mu}}, \quad (24)$$

where multi-index $\tilde{\mu}$ stands for the binary string $\tilde{\mu} = \tilde{\mu}_1 \cdots \tilde{\mu}_N$, with $\mu_i = 0$ or 1, $\forall i \in \mathcal{V}$. Probability $\tilde{P}_{\tilde{\mu}}$ is given simply by the summation of all P_μ in the original Pauli map over all the different events μ for which σ_μ yields—via rules (7)—the same modified operator $Z^{\tilde{\mu}}$ in (24).

To compute the latter modified probability we move to the chord notation [23], mentioned at the end of Sec. II B 1. Indeed, under transformation (7), we have that $T_{i(u_i,v_i)} \rightarrow Z_i^{v_{i1}} \otimes \bigotimes_{j \in \mathcal{N}_i} Z_j^{u_i}$, so that $T_{(U,V)} \equiv T_{1(u_1,v_1)} \otimes \cdots \otimes T_{N(u_N,v_N)} \rightarrow Z_1^{v_1 + \sum_{j \in \mathcal{N}_1} u_j} \otimes \cdots \otimes Z_N^{v_N + \sum_{j \in \mathcal{N}_N} u_j}$. The latter coincides with $Z^{\tilde{\mu}}$ every time $\tilde{\mu}_i = |v_i + \sum_{j \in \mathcal{N}_i} u_j|_2$, $\forall i \in \mathcal{V}$. Thus, in this representation, the modified probability $\tilde{P}_{C\tilde{\mu}}$ is obtained from the defining probability $P_{C(U,V)}$ in the original map by the explicit formula,

$$\tilde{P}_{C\tilde{\mu}} \equiv \sum_U P_{C(u_1, |\tilde{\mu}_1 - \sum_{j \in \mathcal{N}_1} u_j|_2, \ldots, u_N, |\tilde{\mu}_1 - \sum_{j \in \mathcal{N}_N} u_j|_2)}. \quad (25)$$

The modified Kraus operators (24) in turn are fully separable; thus, as said, they trivially satisfy factorization condition (14). We can express them as $\tilde{K}_{\tilde{\mu}} = \tilde{K}_{\mathcal{Y}\tilde{\gamma}} \otimes \tilde{K}_{\overline{\mathcal{Y}}\tilde{\omega}}$, with

$$\tilde{K}_{\mathcal{Y}\tilde{\gamma}} \equiv \tilde{K}_{\mathcal{Y}(\tilde{\gamma}|\tilde{\omega})} = \sqrt{\tilde{P}_{(\tilde{\gamma}|\tilde{\omega})}} Z^{\tilde{\gamma}} \quad \text{and} \quad \tilde{K}_{\overline{\mathcal{Y}}\tilde{\omega}} = \sqrt{\tilde{P}_{\tilde{\omega}}} Z^{\tilde{\omega}}. \quad (26)$$

The new multi-indices are $\tilde{\gamma} = \{\tilde{\mu}_i, i \in \mathcal{Y}\}$ and $\tilde{\omega} = \{\tilde{\mu}_i, i \in \overline{\mathcal{Y}}\}$, and the corresponding probabilities satisfy $\tilde{P}_{(\tilde{\gamma}|\tilde{\omega})} \tilde{P}_{\tilde{\omega}} \equiv \tilde{P}_{\tilde{\mu}}$.

The states $\{\tilde{K}_{\overline{\mathcal{Y}}\tilde{\omega}'}|g_{(\overline{\mathcal{Y}})_0}\rangle = \sqrt{\tilde{P}_{\tilde{\omega}'}} Z^{\tilde{\omega}'}|+\rangle = \sqrt{\tilde{P}_{\tilde{\omega}'}} \bigotimes_{i \in \overline{\mathcal{Y}}} \frac{1}{\sqrt{2}}(|0_i\rangle + (-1)^{\tilde{\mu}_i}|1_i\rangle) \equiv \sqrt{\tilde{P}_{\tilde{\omega}'}}|g_{(\overline{\mathcal{Y}})_{\tilde{\omega}'}}\rangle\}$ are trivially checked to be all orthogonal. Thus, they provide perfect flags that mark each subensemble in the boundary subsystem's ensemble. The perfect flags are revealed by local measurements on the nonboundary qubits in the product basis $\{|g_{(\overline{\mathcal{Y}})_{\tilde{\omega}'}}\rangle\}$. Therefore, for Pauli maps the exact entanglement $E(\rho_t)$ can be calculated by expression (23), which, in terms of binary indices $\tilde{\gamma}$ and $\tilde{\omega}$, and using graph-state relationship (3), can be finally expressed as

$$E(\rho_t) = \sum_{\tilde{\omega}} \tilde{P}_{\tilde{\omega}} E\left(\sum_{\tilde{\gamma}} \tilde{P}_{(\tilde{\gamma}|\tilde{\omega})}|G_{(\mathcal{Y},\mathcal{X})_{\tilde{\gamma}}}\rangle\langle G_{(\mathcal{Y},\mathcal{X})_{\tilde{\gamma}}}|\right), \quad (27)$$

In Fig. 3 we have plotted the bipartite entanglement of the exemplary bipartition of one qubit versus the rest shown in its
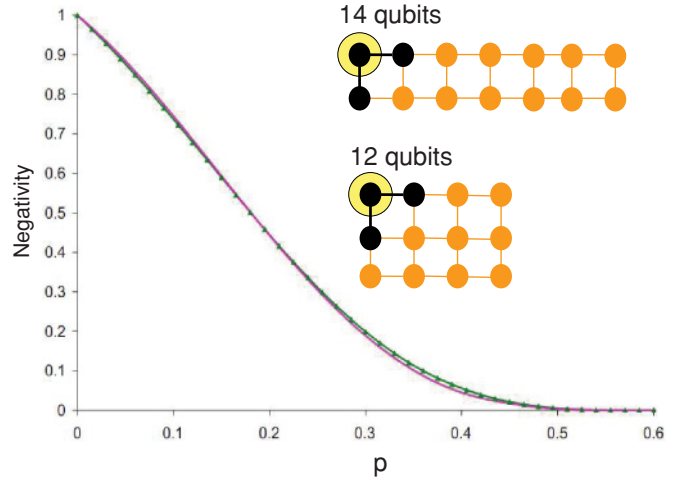

FIG. 3. (Color online) Negativity versus p for 14-qubit (green triangles) and 12-qubit (pink solid curve) cluster states undergoing independent depolarizing noise, and for the bipartition shown in inset. Parameter p can be thought as a parametrization of time (see text).

inset for 14- and 12-qubit graph states evolving under individual depolarization. This map, as said before, is characterized by the one-qubit Kraus operators $\sqrt{1-p}\mathbf{1}, \sqrt{p/3}X, \sqrt{p/3}Y$, and $\sqrt{p/3}Z$. The parameter p ($0 \leqslant p \leqslant 1$) refers to the probability that depolarization has occurred: for $p = 0$ the state is left untouched and for $p = 1$ it is completely depolarized. Once more, p can be also set as a parametrization of time: $p = 0$ referring to the initial time (when nothing has occurred) and $p = 1$ referring to the asymptotic time $t \rightarrow \infty$ (when the system reaches its final steady state).

As the quantifier of entanglement, we choose the negativity [24], defined as twice the absolute value of the sum of the negative eigenvalues of the density matrix partially transposed with respect to the considered bipartition. It is a convex entanglement monotone that in general fails to quantify entanglement of some entangled states—those ones with positive partial transposition (PPT)—in dimensions higher than six [19]. However, since its calculation does not require optimizations but just matrix diagonalizations, it is very well-suited for a simple illustration of our ideas.

We emphasize that, for the 14-qubit graph used in Fig. 3, a brute-force calculation would involve diagonalizing a $2^{14} \times 2^{14} = 16\,384 \times 16\,384$ density matrix for each value of p, whereas with the assistance of expression (27) $E(\rho_p)$ is calculated via diagonalization of at most $2^{11} 2^3 \times 2^3 = 8 \times 8$ dimensional matrices only.

B. Independent thermal reservoirs on graph states

In the case of Pauli maps the entanglement lower and upper bounds coincide, and deliver the exact entanglement. However, this is not the case for general, non-Pauli, noise channels. The upper bound is given, as usual, by convexity. The lower bounds must be optimized by appropriately choosing the LOCC operations. Here, we investigate and optimize measurement strategies for channel GAD, defined in Sec. II B 2.

Observe that the Kraus operators defined in Eq. (10) satisfy the following: K_{i0} and K_{i2} commute with any CZ operator, while for every $j \in \mathcal{V}$ different from i it holds
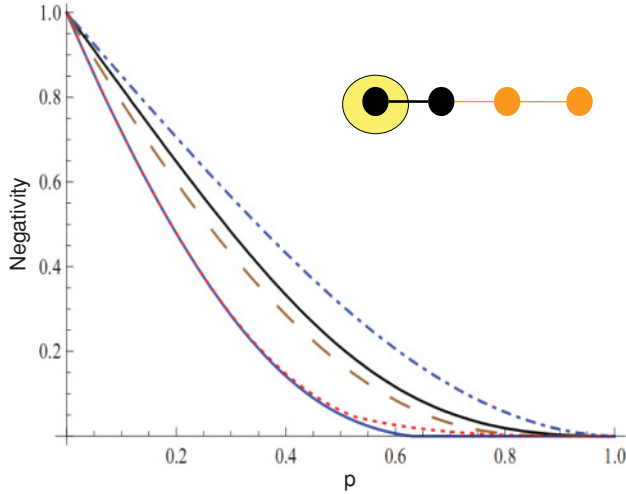
FIG. 4. (Color online) Negativity versus p for a four-qubit linear cluster subjected to the amplitude damping channel and for the partition displayed in the inset. Solid (upper) black curve, exact entanglement; solid (lower) blue curve, lowest lower bound LLB (obtained by tracing out the flags); dashed-dotted blue curve, upper bound (obtained by convexity); dotted red curve, LB(0) (obtained by measuring the flags in the Z basis); dashed brown curve, LB($\pi/4$) (obtained by measuring the flags in the X basis).

that $(K_{i1} \otimes \mathbf{1}_j) \cdot CZ_{ij} = CZ_{ij} \cdot (K_{i1} \otimes Z_j)$ and $(K_{i3} \otimes \mathbf{1}_j) \cdot CZ_{ij} = CZ_{ij} \cdot (K_{i3} \otimes Z_j)$. Based on this, one can perform the factorization in equation (13) and apply this way the formalism described in Sec. III A.

In what follows we focus on two main limits of channel GAD discussed in Sec. II B 2: the purely dissipative limit $\overline{n} = 0$ (amplitude damping), and the purely diffusive limit $\overline{n} \to \infty$, $\gamma \to 0$, and $\overline{n}\gamma = \Gamma$.

1. Graph states under zero-temperature dissipation

We consider a four-qubit linear (one-dimensional) cluster state subjected to the AD map and study the decay of entanglement in the partition consisting of the first qubit versus the rest shown in the inset of Fig. 4. Along with the exact calculation of entanglement via brute-force diagonalization of the partially transposed matrices, the lowest lower bound LLB (20), obtained by tracing out the flags, and the upper bound (22), obtained from convexity, are plotted. In addition, the tightness of the lower bounds (18) obtained by the flag measurements can be scanned as a function of the measurement bases.

Based on observations about the behavior of the system under the AD map we can guess good measurement strategies. For example, examination of the initial state reveals that at $p = 0$ each of the nonboundary qubits is in one of the states of the basis $\{|+\rangle, |-\rangle\}$; whereas at $p = 1$, in one of the states of $\{|0\rangle, |1\rangle\}$. We call the lower bound obtained from (18) through measurements in the basis $\{|+\rangle, |-\rangle\}$ LB($\pi/4$), and the one obtained from (18) through measurements in $\{|0\rangle, |1\rangle\}$ LB(0). The latter bounds are the two additional curves plotted in Fig. 4. We observe that LB(0) provides only a slight improvement over the LLB, whereas LB($\pi/4$) appears to give a significant one. This raises the obvious question of how to optimize the choice of measurement basis at each instant p in the evolution.
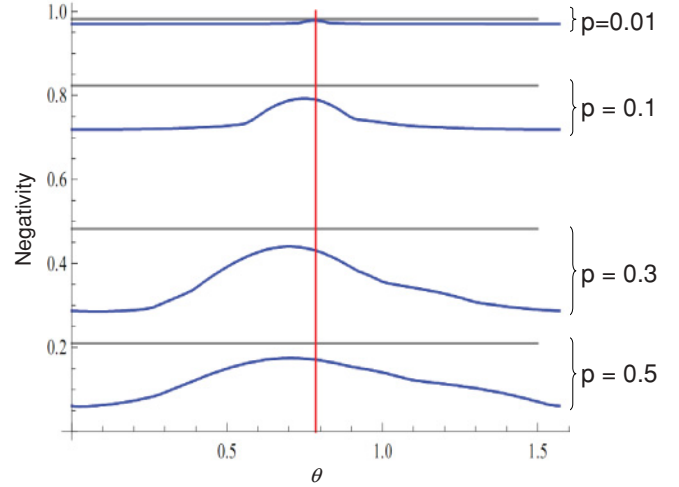

FIG. 5. (Color online) Lower bound LB(θ) to the negativity as a function of the angle θ in the measurement basis, for the same situation as in Fig. 4, and for fixed values of p. Each value $p = 0.01, 0.1, 0.3, 0.5$ has two curves associated with it. The horizontal (gray) straight line represents the exact entanglement at each p, while the blue (black) curve represents the bound LB(θ) at this p. The red line (vertical) corresponds to $\theta = \frac{\pi}{4}$ (i.e., measurements in the basis $\{|+\rangle, |-\rangle\}$).

As an illustration we consider lower bounds LB(θ) obtained from (18) through orthogonal measurements composed of projectors $|\theta+\rangle = \cos\theta|0\rangle + \sin\theta|1\rangle$ and $|\theta-\rangle = -\sin\theta|0\rangle + \cos\theta|1\rangle$, and look for the angle θ that gives us approximately the largest value of LB(θ). This is certainly not the most general measurement scenario one may consider, but it gives one a hint on how to increase the tightness of the bounds.

Figures 5 and 6 illustrate this idea. At fixed values of p, we have varied angle θ in the range $[0, \pi/2]$. The entanglement given by LB(θ) for each value of θ is compared with the exact entanglement at the given p. In physical terms, we are taking snapshots of the evolution of the system's entanglement at discrete time instants. The value of θ at each instant p that maximizes LB(θ) represents the optimal measurement
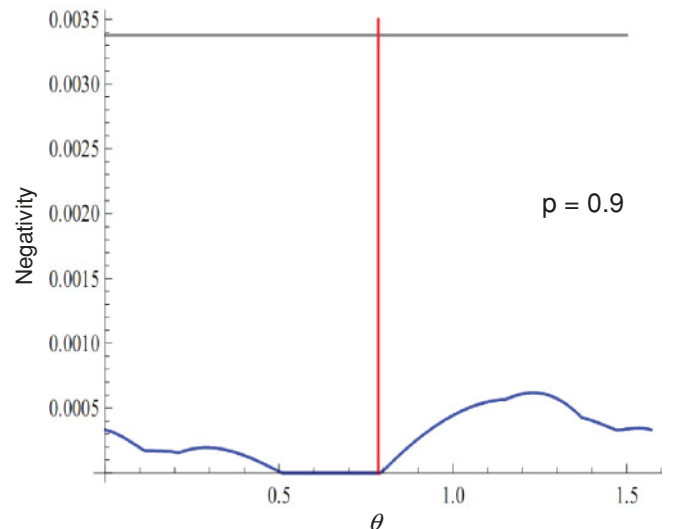

FIG. 6. (Color online) Same as Fig. 5 for $p = 0.9$.

basis at that particular instant. As is clearly seen in Fig. 5, for small values of p angles around $\theta = \frac{\pi}{4}$ give the closest approximations to the exact entanglement, in consistence with the significant improvement of LB($\pi/4$) over the LLB observed in Fig. 4. For large values of p though, the best approximations tend to be given by the angles away from $\theta = \frac{\pi}{4}$, as can be observed in Fig. 6. It must still be kept in mind that none of these closest approximations equals the exact entanglement of the state.

2. Graph states under infinite-temperature diffusion

We now consider the purely diffusive case of the GAD channel, where each qubit is in contact with an independent bath of infinite temperature. In Fig. 7 we display the entanglement evolution in a similar way as in Fig. 4. Since in the purely diffusive limit channel GAD becomes a Pauli map, as was mentioned in the end of Sec. II B 2, bound LB($\pi/4$) yields the exact entanglement. LB(0) on the other hand coincides with the lowest lower bound LLB. The fact that in this case LB(θ) reaches the exact entanglement at $\theta = \frac{\pi}{4}$ can also be seen in a clearer way in Fig. 8.

In Fig. 7 the upper bound (22) is plotted as well. Since in this case the channel is a Pauli channel, one would expect the upper bound to coincide with the exact entanglement as well. The fact that this does not occur is because, even though the noise itself is describable as a Pauli map, the plotted upper bound has been calculated using the original Kraus decomposition of Eq. (10), which is not in a Pauli-map form. For every given particular Kraus decomposition of a superoperator, the naive application of convexity always yields UB through Eq. (22), but this needs not the tightest, for the Kraus decomposition of a superoperator is in general not unique. This observation leads to a whole family of upper bounds for a given map. In the same

FIG. 8. (Color online) Lower bound LB(θ) to the negativity as a function of the angle θ in the measurement basis, for the same situation as in Fig. 7, and for fixed values of p. Each value $p = 0.01, 0.1, 0.3, 0.5$ has two curves associated with it. Again, the horizontal (gray) straight line represents the exact entanglement at each p, while the blue (black) curve represents the bounds LB(θ) at this p. The red line (vertical) corresponds to $\theta = \frac{\pi}{4}$ (i.e., measurement in the basis $\{|+\rangle, |-\rangle\}$).

spirit as with the lower bounds, one could in principle optimize the obtained UBs over all possible Kraus representations of the map.

V. EXTENSIONS AND LIMITATIONS

The framework developed here is not restricted to graph states. The crucial ingredient in our formalism is to factor out all the entangling operations that act as local unitary transformations with respect to the considered partition, and to redefine the Kraus operators acting on the state, reducing the entanglement evaluation problem to the boundary subsystem alone. Given an entangled state and a prescription for its construction in terms of entangling operations, useful bounds and exact expressions for the entanglement can be readily obtained. As an example, a GHZ-like state $|\psi\rangle = \alpha|0\rangle^{\otimes N} + \beta|1\rangle^{\otimes N}$ can be operationally constructed by the sequential application of the maximally entangling operation controlled-NOT $(\text{CNOT})_{ij} = |0_i 0_j\rangle\langle 0_i 0_j| + |0_i 1_j\rangle\langle 0_i 1_j| + |1_i 0_j\rangle\langle 1_i 1_j| + |1_i 1_j\rangle\langle 1_i 0_j|$ to the product state $(\alpha|0\rangle + \beta|1\rangle) \otimes |0\rangle \otimes \cdots \otimes |0\rangle$ such that $|\psi\rangle = \bigotimes_{i=1}^{N-1} \text{CNOT}_{i,i+1}(\alpha|0\rangle + \beta|1\rangle) \otimes |0\rangle \otimes \cdots \otimes |0\rangle$. Using our techniques and the permutation symmetry of the state it can be seen that, for GHZ-like states undergoing the previously discussed noise processes, the entanglement evaluation in any bipartition can be reduced to that of a two-qubit system. It is also important to mention that the techniques presented here can also be straightforwardly extended to higher-dimensional graph states [25].

In addition, it is important to mention that all bounds developed so far can in fact also be exploited to follow the entanglement evolution when the system's initial state is a mixed graph-diagonal state. This is simply due to the fact that
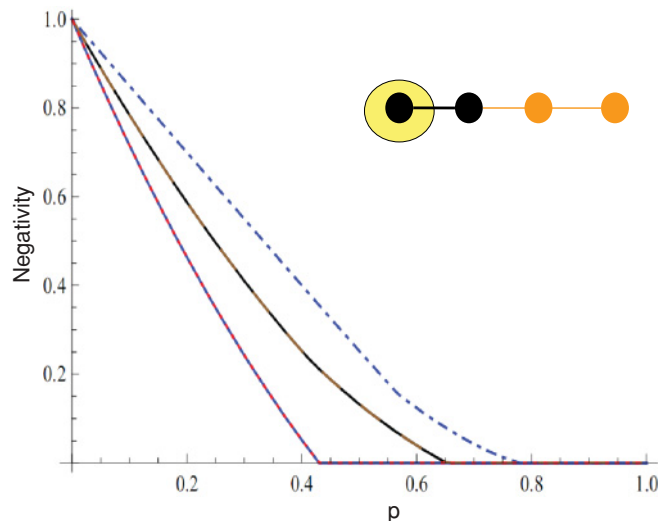

FIG. 7. (Color online) Negativity versus p for a four-qubit linear cluster for the bipartition shown in the inset, subjected to the generalized amplitude damping channel in the diffusive limit $\bar{n} \to \infty$. The central curve corresponds to both the exact entanglement (solid black) and LB($\pi/4$) (dashed brown), which coincide exactly. The lower curve corresponds to both LBB (solid blue) and LB(0) (dotted red), which also coincide exactly. The upper curve is the upper bound (22) (dot-dashed blue).
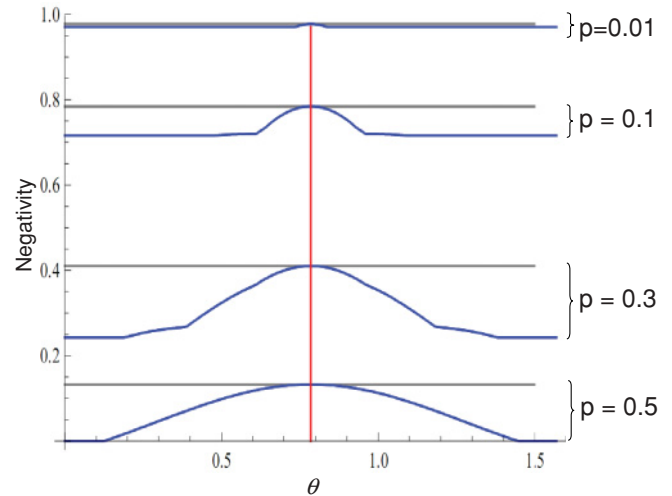
any graph-diagonal state as (4) can be thought of as a Pauli map Λ_{GD} acting on a pure graph state:

$$\rho_{GD} = \sum_{\nu} P_{\nu} |G_{(\mathcal{V},\mathcal{C})_{\nu}}\rangle\langle G_{(\mathcal{V},\mathcal{C})_{\nu}}|$$

$$= \sum_{\nu} P_{\nu} Z^{\nu} |G_{(\mathcal{V},\mathcal{C})_0}\rangle\langle G_{(\mathcal{V},\mathcal{C})_0}| Z^{\nu} = \Lambda_{GD}\big(|G_{(\mathcal{V},\mathcal{C})_0}\rangle\big).$$

(28)

Thus, the entanglement at any time t in a system initially in a mixed graph-diagonal state ρ_{GD}, and evolving under some map Λ, is equivalent to that of an initial pure graph state $|G_{(\mathcal{V},\mathcal{C})_0}\rangle$ whose evolution is ruled by the composed map $\Lambda \circ \Lambda_{GD}$, where Λ_{GD} is defined in (28). When Λ is itself a Pauli map, then $\Lambda \circ \Lambda_{GD}$ is also a Pauli map and the expression (27) for the exact entanglement can be applied. For the cases where Λ is not a Pauli map but the relations (13) are satisfied by its Kraus operators, the relations (13) will also be satisfied by the composed map $\Lambda \circ \Lambda_{GD}$, so that all other bounds derived here also hold.

Furthermore, as briefly mentioned before, any arbitrary state can be depolarized by some separable map toward a graph-diagonal state without changing the diagonal elements in the considered graph basis [21]. The latter, since the entanglement of almost all states cannot increase under separable maps [26], implies that all the lower bounds presented here also provide lower bounds to the decay of the entanglement that, though in general far from tight, apply to almost any arbitrary initial state subject to any decoherence process.

The gain in computational effort provided by the machinery presented here diminishes with the ratio between the number of particles in the boundary subsystem and the total number of particles. For example, for multipartitions such that the boundary system is the total system itself, or for entanglement quantifiers that do not refer to any multipartition at all, our method yields no gain. An example of the latter are the entanglement measures that treat all parties in a system indistinguishably, some of which, as was mentioned in Sec. I,

have been studied in Refs. [15,16]. These methods naturally complement with ours to offer a rather general and versatile toolbox for the study of the open-system dynamics of graph-state entanglement.

VI. CONCLUSIONS

We have studied in detail a general method for computing the entanglement of graph and graph-diagonal states undergoing decoherence, introduced in Ref. [17]. This method allows one to drastically reduce the effort to compute the entanglement evolution of graph states in several physical scenarios. We have given an explicit formula for the construction of the effective noise involved in the calculation for Pauli maps and extended the formalism to the case of independent baths at arbitrary temperature. Furthermore, we have elaborated the formalism to construct nontrivial lower and upper bounds to the entanglement decay where exact results cannot be obtained from the formalism itself.

Finally, we would like to add that the necessary requirements on the noise channels for the method to apply do not prevent us from obtaining general results for a wide variety of realistic decoherence processes. Furthermore, the conditions required on the entanglement measures are satisfied by most quantifiers.

[1] M. Hein, J. Eisert, and H. J. Briegel, Phys. Rev. A **69**, 062311 (2004); M. Hein, W. Dür, J. Eisert, R. Raussendorf, M. Van den Nest, and H. J. Briegel, *Proceedings of the International School of Physics Enrico Fermi on "Quantum Computers, Algorithms and Chaos"* (2006), e-print arXiv:quant-ph/0602096.

[2] R. Raussendorf and H. J. Briegel, Phys. Rev. Lett. **86**, 5188 (2001); R. Raussendorf, D. E. Browne, and H. J. Briegel, Phys. Rev. A **68**, 022312 (2003).

[3] H. J. Briegel, D. E. Browne, W. Dür, R. Raussendorf, and M. Van den Nest, Nature Phys. **5**, 19 (2009).

[4] D. Schlingemann and R. F. Werner, Phys. Rev. A **65**, 012308 (2001).

[5] W. Dür, J. Calsamiglia, and H. J. Briegel, Phys. Rev. A **71**, 042336 (2005); K. Chen and H.-K. Lo, Quantum Inf. Comput. **7**, 689 (2007).

[6] O. C. Dahlsten and M. B. Plenio, Quantum Inf. Comput. **6**, 527 (2006).

[7] D. M. Greenberger, M. A. Horne, and A. Zeilinger, in *Bell's Theorem, Quantum Theory, and Conceptions of the Universe*, edited by M. Kafatos (Kluwer, Dordrecht, 1989), p. 69.

[8] S. Bose, V. Vedral, and P. L. Knight, Phys. Rev. A **57**, 822 (1998); M. Hillery, V. Bužek, and A. Berthiaume, *ibid.* **59**, 1829 (1999); E. D'Hondt and P. Panangaden, Quantum Inf. Comput. **6**, 173 (2005).

[9] V. Giovannetti, S. Lloyd, and L. Maccone, Science **306**, 1330 (2004).

[10] J. Bollinger, W. M. Itano, D. Wineland, and D. Heinzen, Phys. Rev. A **54**, R4649 (1996).

[11] P. Walther *et al.*, Nature **434**, 169 (2005); N. Kiesel, C. Schmid, U. Weber, G. Toth, O. Guhne, R. Ursin, and H. Weinfurter, Phys. Rev. Lett. **95**, 210502 (2005); C. Y-. Lu *et al.*, Nature Phys. **3**, 91 (2007); K. Chen, C. M. Li, Q. Zhang, Y. A. Chen, A. Goebel, S. Chen, A. Mair, and J. W. Pan, Phys. Rev. Lett. **99**, 120503

(2007); G. Vallone, E. Pomarico, F. DeMartini, and P. Mataloni, *ibid.* **100**, 160502 (2008).

[12] C. Simon and J. Kempe, Phys. Rev. A **65**, 052327 (2002).

[13] W. Dür and H.-J. Briegel, Phys. Rev. Lett. **92**, 180403 (2004); M. Hein, W. Dür, and H.-J. Briegel, Phys. Rev. A **71**, 032350 (2005).

[14] L. Aolita, R. Chaves, D. Cavalcanti, A. Acín, and L. Davidovich, Phys. Rev. Lett. **100**, 080501 (2008); L. Aolita, D. Cavalcanti, A. Acín, A. Salles, Markus Tiersch, A. Buchleitner, and F. de Melo, Phys. Rev. A **79**, 032322 (2009).

[15] O. Gühne, F. Bodoky, and M. Blaauboer, Phys. Rev. A **78**, 060301 (2008).

[16] H. Wunderlich, S. Virmani, and M. B Plenio, e-print arXiv:1003.1681.

[17] D. Cavalcanti, R. Chaves, L. Aolita, L. Davidovich, and A. Acín, Phys. Rev. Lett. **103**, 030502 (2009).

[18] G. Vidal, J. Mod. Opt. **47**, 355 (2000).

[19] M. B. Plenio and S. Virmani, Quantum Inf. Comput. **7**, 1 (2007); R. Horodecki, P. Horodecki, M. Horodecki, and K. Horodecki, Rev. Mod. Phys. **81**, 865 (2009).

[20] D. Cavalcanti, L. Aolita, A. Ferraro, A. Garcia-Saez, and A. Acín, New J. Phys. **12**, 025011 (2010).

[21] W. Dür, H. Aschauer, and H. J. Briegel, Phys. Rev. Lett. **91**, 107903 (2003); H. Aschauer, W. Dür, and H. J. Briegel, Phys. Rev. A **71**, 012319 (2005).

[22] M. A. Nielsen and I. L. Chuang, *Quantum Computation and Quantum Information* (Cambridge University Press, Cambridge, 2000).

[23] M. L. Aolita, I. García-Mata, and Marcos Saraceno, Phys. Rev. A **70**, 062301 (2004).

[24] G. Vidal and R. F. Werner, Phys. Rev. A **65**, 032314 (2002).

[25] D. L. Zhou, B. Zeng, Z. Xu, and C. P. Sun, Phys. Rev. A **68**, 062303 (2003); M. S. Tame, M. Paternostro, C. Hadley, S. Bose, and M. S. Kim, *ibid.* **74**, 042330 (2006).

[26] Separable maps cannot increase entanglement when acting on pure states [see V. Gheorghiu and R. B. Griffiths, Phys. Rev. A **78**, 020304(R) (2008)]; or on general separable states, of course. However, pathologic examples have been found of mixed entangled states for which the value of some particular entanglement monotone can increase under separable maps [see E. Chitambar and R. Duan, Phys. Rev. Lett. **103**, 110502 (2009)].